

# Pulse width dependent dynamics of laser-induced plasma from a Ni thin film

Jinto Thomas<sup>1,2</sup>, Hem Chandra Joshi<sup>1,3</sup>, Ajai Kumar<sup>1,3</sup> and Reji Philip<sup>4</sup>

<sup>1</sup> Institute For Plasma Research, Bhat, Gandhinagar, Gujarat, 382428, India

<sup>2</sup> Nirma University, Ahmedabad, Gujarat, 382421, India

<sup>3</sup> Homi Bhabha National Institute, Training School Complex, Anushakti Nagar, Mumbai 400085, India

<sup>4</sup> Raman Research Institute, Sadashiva nagar, Bangalore, 560080, India

E-mail: [jjinto@ipr.res.in](mailto:jjinto@ipr.res.in)

Received 3 October 2018, revised 17 December 2018

Accepted for publication 7 January 2019

Published 1 February 2019



## Abstract

Plasma plume formation and its expansion in the background gas are investigated in a 50 nm thick Ni thin film under the rear ablation/laser blow-off (LBO) geometry, employing 10 ns, 200 ps and 100 fs laser pulses respectively. Plume directionality, splitting and expansion are found to depend on the laser pulse width, and the expansion behavior is explained by appropriate models. In the case of fs ablation, the plume shows a linear expansion at lower background pressures, while at higher pressures the expansion appears to show shock wave like nature. For ps ablation the expansion appears to follow a blast wave model at lower pressures, which, however, fits with drag model at higher pressures. In case of ns ablation, shock wave like nature is observed for all the pressures. Further, we believe the present study may have potential implications in pulsed laser deposition, ultra fast laser based nano particle generation and micro-machining.

Keywords: laser ablation, drag model, plasma plume dynamics, plume imaging, blast model

(Some figures may appear in colour only in the online journal)

## 1. Introduction

Ablation of solid targets by an intense laser pulse and subsequent propagation of the laser-induced plasma plume in the surrounding gas medium have attracted substantial research interest in recent times. Light-matter interaction, especially laser ablation and plume propagation, has been investigated in the past for metals, semiconductors, and polymers [1, 2]. The dynamics and properties of the plasma plume formed by laser irradiation of a given target essentially depend on the material properties, the surrounding medium into which it expands, experimental geometry, and the laser beam characteristics. Kumar *et al* [3] studied the effect of spatial energy distribution of the laser pulse on plume propagation in a laser blow-off experiment using nanosecond pulses to ablate a thin film. They found that a Gaussian spatial profile produces a well-collimated, low divergence plasma plume, as compared to the plume formed by a top-hat profile. Yeates *et al* [4] studied the dynamics of aluminium plasma plume generated by nanosecond pulses, expanding between confining surfaces.

Michael *et al* [5] discussed the collimation of a dense plasma jet generated by picosecond laser pulses on triangular grooved cavities. Amoroso *et al* [6] reported the experimental characterization and theoretical analysis of ultrashort laser ablation of a nickel target.

The processes involved in plasma plume formation depend largely on the fluence, excitation wavelength and pulse width of the laser source used for ablation [7, 8]. In most of the conventional studies, the laser produced plasma (LPP)/front ablation geometry, where the laser beam is focused on a solid target either normal to the surface or at an angle, is used for the generation of the plasma plume. The generated plume expands in the surrounding gas or vacuum, while interacting with the ablating laser pulse in some cases, depending on the laser pulse width. Rear ablation/laser blow-off (LBO) is another geometry used for tokamak plasma diagnostics [9, 10], transport studies [11], thin film deposition and in semiconductor industry [12]. Here the ablating laser pulse reaches the thin film sample after passing the substrate, such that the plume/material expands in the forward direction along the

laser (refer to [13]). This technique has the advantage that the plasma plume can produce a particle beam with a significant percentage of neutrals in it [14] which is helpful in plasma diagnostics. The pulse width of the laser plays an important role in the ejection of material and hence plume expansion [15–17]. In ns regime the dominant process is melting and subsequent vaporization, whereas in the femtosecond regime processes like Coulomb explosion dominate [18, 19].

Although there are several works on front ablation using pulse widths from femto second to nanosecond [17, 20, 21], in the case of rear ablation only limited studies are reported [22, 23]. Recently it has been reported that rear ablation geometry is more favorable for cleaning of transparent objects as well as in thin film deposition [23–26]. Hence a comparative study of the same target using laser pulses with varying pulse widths exploiting rear/front ablation is essentially an important aspect for various applications. LPP studies on nickel has been done by some groups [6, 24] however, ablation studies on nickel thin film are limited to a few [23, 25, 27]. The present work is an investigation of the expansion dynamics of LBO plasma plumes generated from a nickel thin film (50 nm) using laser pulses of comparable optical fluence but different excitation pulse widths (10 ns, 200 ps and 100 fs respectively). We show that there exists a distinct relationship between the dynamics of plume expansion in the background medium (in this work  $N_2$ ) and the ablation laser pulse width.

## 2. Experimental set-up

The experimental set up is similar to that reported in some earlier LBO reports [13] except for the laser. The excitation source is a femto second CPA amplifier system with 86 MHz titanium sapphire seed laser and 10 Hz chirped pulse amplifier (TSA-10, positive light). Inside the TSA-10, the seed pulse is stretched in time to nearly 200 ps, prior to amplification. The amplifier is pumped by the second harmonic output (532 nm) of a Q-switched Nd:YAG laser running at 10 Hz. The fundamental residue of the Nd:YAG laser after the generation of second harmonic is safely dumped. Outputs from different stages of laser amplifier system are used for generating the plasma. Pulses of 10 ns are obtained from the fundamental output (1064 nm) of the pulsed Nd:YAG laser which pumps the CPA amplifier. The temporally chirped laser pulse in the amplifier has a pulse width of 200 ps, while the final amplifier output after pulse compression has a pulse width of 100 fs. The maximum output energy available for fs and ps pulses is 10 mJ per pulse. The laser beam path is aligned through multiple apertures so that the laser pulses trace the same path, and the position of plasma plume formation is not altered when using different laser pulses.

The thin film used for this study is of nickel with thickness of 50 nm, and is coated on a quartz substrate. The thin film is mounted on a vacuum compatible  $x$ - $y$  translator for positioning it at the focal point of the laser beam. Care is taken that the laser pulses do not ablate the substrate (glass) significantly. This is confirmed by acquiring the ICCD images by replacing the sample with a similar glass slide. Also, the ICCD images

**Table 1.** Table showing the laser beam parameters for three different pulsewidths used.

Sr. No.	Pulse width	Wavelength (nm)	Spot diameter (mm)	Laser energy (mJ)
1	100 fs	800	0.8	8.0
2	200 ps	800	0.8	8.0
3	8 ns	1064	1.1	30.0

do not show any plasma plume in the direction opposite to the laser, indicating that the substrate is not ablated. The laser beam parameters and spot sizes are listed in table 1. As is evident from the table, for picosecond and femtosecond cases, laser energy, spot diameter as well as wavelength are same although for ns case there is some difference in laser energy and spot size (due to the wavelength difference). However, overall fluence is not much affected ( $\approx 3 \text{ J cm}^{-2}$  in case on nanosecond and  $2 \text{ J cm}^{-2}$  in case of picosecond and femtosecond). Moreover the wavelength is also not too much different (1064 nm in case of nanosecond and 800 nm in case of picosecond and femtosecond). Based on these parameters a relative comparison appears reasonable.

In addition to the ICCD camera, a high resolution spectrometer (iHr320) with PMT is used for recording spectral lines emitted from the plasma. An imaging system with two lenses images a small portion of the plasma directly on the slit of the spectrometer. The spectra from multiple spatial locations are recorded on a shot to shot basis with multiple averaging. The vacuum vessel is evacuated up to a base value of  $5 \times 10^{-6}$  mbar and then  $N_2$  gas is filled up to the desired background pressure with the help of a precision leak valve. A fast photo diode near the focusing lens provides trigger for the ICCD and also records the zero time for the measurement. The sync out pulse corresponding to the gating time is used to measure the delay of exposure. A triple Langmuir probe (TLP) [28] is used to measure the ion saturation current at a distance of 10 mm from the sample.

## 3. Results and discussion

Figure 1 shows plume images recorded within a time of 100 ns–1  $\mu$ s after the irradiation, using an ICCD with gating time of 50 ns for different laser pulse widths and pressure. It is clearly evident from the images that the plasma plume dynamics is distinctly different for different laser pulse widths for a given background pressure. The plasma plume evolution is also distinct for each background pressure. The scenario can be described as follows: (i) in femto-second excitation (figure 1(a)), the plume breaks into two components (fast and slow) and gets well separated during propagation. The separation between the two broken components monotonically increases as the plume propagates against the background pressure of  $5 \times 10^{-2}$  mbar. However, as the background pressure increases, the separation between the fast and slow components decreases as can be seen in the figure for 1 mbar background pressure. Interestingly, fast images at 10 mbar of background pressure do not show any signature of plume splitting. (ii) In the case of ps ablation (figure 1(b)),

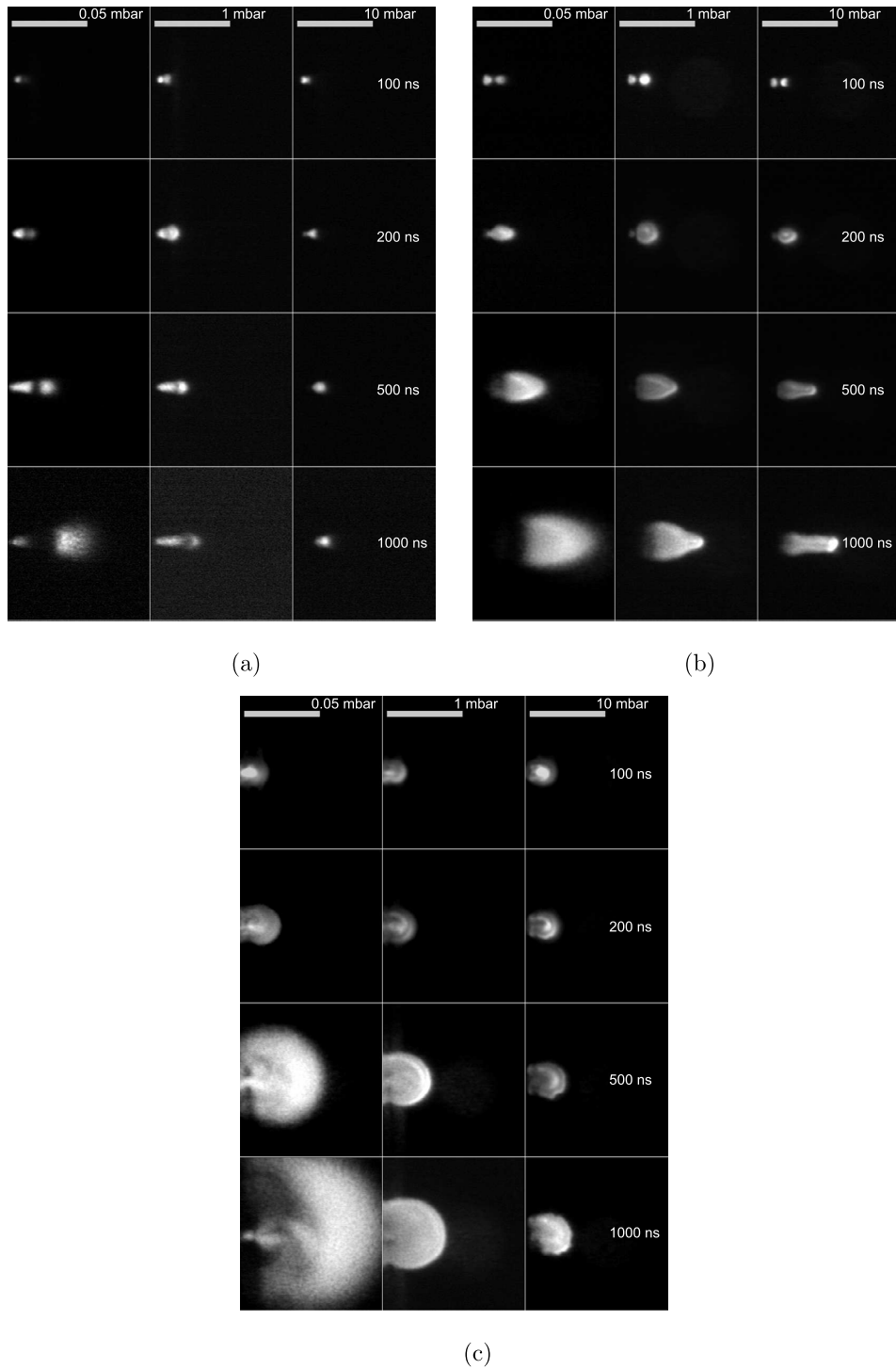


**Figure 1.** Temporal evolution of the rear ablated nickel plasma plume generated in a 50 nm thick Ni thin film using three different laser wavelengths and pulse widths, viz. 800 nm 100 fs, 800 nm 200 ps and 1064 nm 10 ns. The plume expands into a nitrogen background of pressure  $5 \times 10^{-2}$  mbar, 1.0 mbar and 10 mbar. ICCD gate width is 50 ns, and the duration of measurement is 2  $\mu$ s. (a) 800 nm 100 fs. (b) 800 nm 200 ps. (c) 1064 nm 10 ns.

the plasma plume initially shows splitting irrespective of the background pressure. However, as the time increases, the fast component propagates and the slow portion fades out. As the background pressure increases to 10 mbar, the plasma plume shows highly directional expansion. (iii) For nanosecond ablation (figure 1(c)), it can be seen that the plume expands almost spherically without splitting and with increase in background

pressure, the plume is confined circularly in contrast to the femto-second and pico-second generated plasma plumes.

With 50 ns ICCD gating, for ps and fs ablation, plume intensity falls below the detection limit of the camera at about 1  $\mu$ s after laser irradiation. However, the plume images recorded using the gate width of 250 ns, for 1 mbar of background pressure, show that the emission from plasma plume is

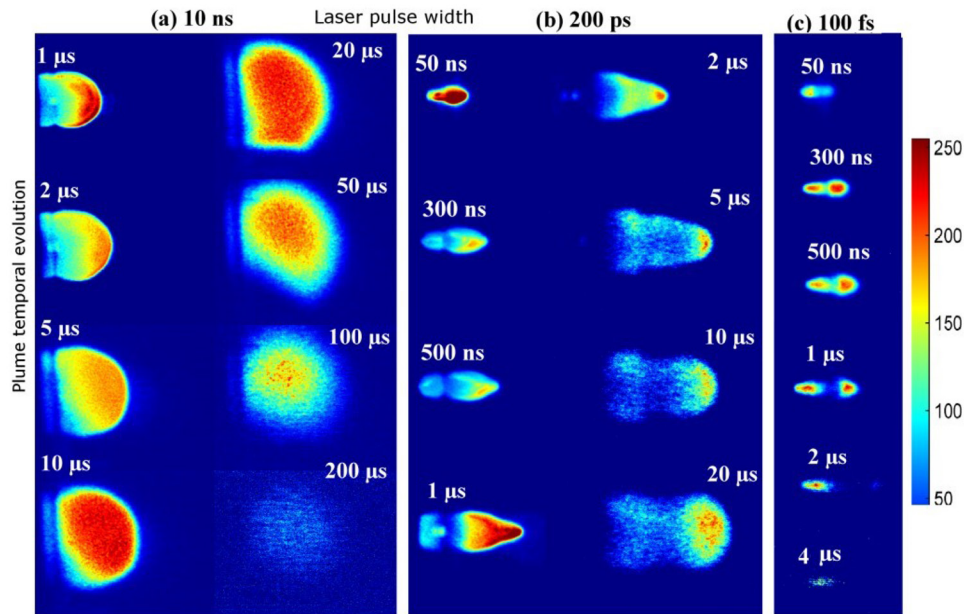


**Figure 2.** ICCD images recorded with 250 ns gating for 10 ns, 200 ps and 100 fs ablation for 1 mbar of background pressure. Each image is normalized to its maximum intensity for better visibility. (a) 10 ns. (b) 200 ps. (c) 100 fs.

visible for nearly 200  $\mu$ s, 10  $\mu$ s and 4  $\mu$ s, for the 10 ns, 200 ps and 100 fs pulses respectively, as can be seen in figure 2. The plume formed by nanosecond ablation develops into complete spherical shape as shown in figure 2(a). The plume boundary is distinct up to about 10  $\mu$ s, beyond which it diffuses. The spatial evolution of the plume disappears at around 50  $\mu$ s and the emission intensity starts diminishing. However, the plumes formed by 200 ps and 100 fs pulses show distinctly different behaviour in the later part of their expansion. With ps excitation, in addition to the initial splitting, the plume focuses and then further splits into two segments, as is evident from figure 2(b). Figure 2(c) shows plume expansion up to 4  $\mu$ s for the plume formed with 100 fs ablation, where the plume splitting can be clearly seen from about 300 ns itself.

This plume splitting phenomenon can be attributed to the generation of fast and slow components in the plume due to the presence of ions as well as neutrals as has been reported in a number of earlier works [29–31]. It has been reported that ions are accelerated inside the plasma by the ambipolar electric field due to the plasma multi layer giving rise to faster component consisting of ions. At later times due to decrease in temperature, recombination may take place resulting in neutrals and hence fast component will vanish. We found that in the case of fs generated plume, the fast component vanishes quickly in comparison to the slow component. This observation is in line with earlier laser-produced plasma work [32], where nano-particle formation is reported for carbon plasma.

Another interesting observation here is the lack of plume splitting in the case of nanosecond ablation. This indicates that the constituents of the plasma plume (ions and/or neutrals) formed by nanosecond ablation travel with almost the same velocity, unlike in the case of pico second and femto second ablations. The absence of fast and slow components in ns generated plasma plume can be understood by the fact that in ns plasma the plasma may get heated by the inverse

bremstrahlung (IB) process in the initial stages. The IB process heats the plasma resulting in higher temperature and density. Due to this increased density and temperature, the extent of ionization will be much larger and the contribution of neutrals inside the plume will be limited. From this, one can predict that the major constituent of the plume should be ionized species which get accelerated. Here we would like to mention that the ion current measured using TLP for a background pressure of  $5 \times 10^{-2}$  mbar at 10 mm from the sample shows that the relative value of the current in the case of ns produced plasma is  $\approx 62$  times more than that in case of fs plasma and  $\approx 13$  times more than that of the ps plasma (not shown). The TLP measurements also show that the peaking times of the ion current are 0.7  $\mu$ s, 0.84  $\mu$ s and 1.3  $\mu$ s for ns, ps and fs generated plasma plumes respectively. A similar trend in ion current measurements is observed for other background pressures also. However, at higher background pressures the ion current becomes negligible at 10 mm from the sample for ps and fs generated plasma plumes. Interestingly spectroscopic observations show (figure 3) strong neutral emission, which of course, can be attributed to the recombination process, occurring under these conditions. Hence, spectroscopic evolution is used to explore the dynamics of neutrals in the plume using a prominent nickel line of 361.9 nm. The dynamics of neutral nickel is studied for all the three pulse widths using the spectroscopic time of flight (TOF) signal.

Figure 3 shows the TOF signals recorded with spectrometer and PMT at a background pressure of  $5 \times 10^{-2}$  mbar and 1 mbar for three different pulse widths at 5 mm from the sample. It can be seen that the background pressure does not significantly change the time of arrival for nanosecond and pico second ablations, however, the plume formed due to the fs ablation has a significant difference in signal intensity as well as in the time of arrival. At 1.0 mbar, the intensity of the neutral line for the plume is very small and plume speed is slower



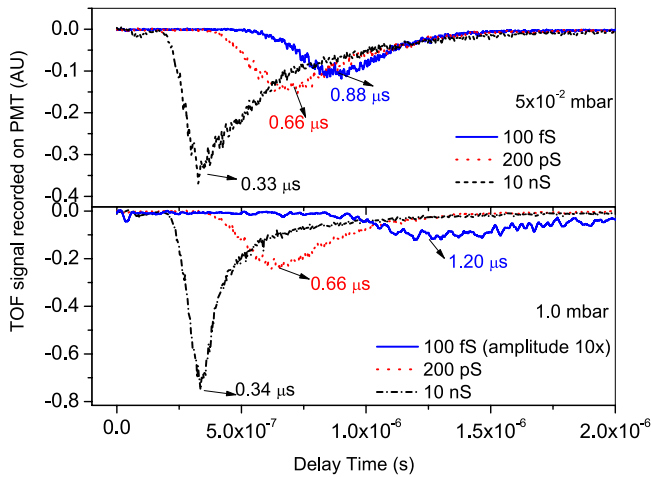


**Figure 3.** Comparison of emission front of neutral line (361.9 nm) recorded using spectrometer and PMT for  $5 \times 10^{-2}$  mbar and 1.0 mbar for three different pulse widths at 5 mm from the sample.

compared to that at  $5 \times 10^{-2}$  mbar. The emission intensity falls significantly and is beyond the measurement limit for 10 mbar of background pressure. At a given pressure, the arrival times from spectroscopic observation of neutral lines as well as from the ion current measurements show that the nanosecond laser generated plasma plume has significantly larger velocity as compared to the plume formed by pico second and femto second laser pulses. These observations further support the argument that ions are dominant in the case of ns excitation which convert into neutrals after recombination and hence no signature of plume splitting is evident. The slower velocity for femto second generated plasma plume suggests the formation of massive plume constituents, e.g. nano-particles which is in line with earlier report [33].

Figure 4 is a comparison of time of arrival of plume front estimated from the ICCD images with the spectra recorded using the spectrometer and PMT. It can be noted that for the nanosecond laser generated plasma the position of plasma plume front and that of the neutral emission match well. Again this shows that the velocity of neutral species as well as the whole species in plume front (image) is the same. Hence, as mentioned earlier we can anticipate that the origin of neutrals and the ions should be the same and lies in the ion formation. In the temperature range of nanosecond laser generated plasma (more than 1.5 eV), as mentioned earlier, the extent of ionization is very high and has a large portion of ions [34]. Again, earlier the velocity of neutrals is the same as that of the plasma plume, confirming that the neutrals are generated from the ions due to recombination process. In the case of pico-second laser produced plasma, there is a significant lag in the time between the plasma plume front estimated from fast imaging as compared to the emission of the neutrals as seen from figure 4 for background pressures of  $5 \times 10^{-2}$  mbar and 1.0 mbar. Fast imaging (figure 1) shows a plume splitting initially which, however, is not seen in the TOF spectrum of neutrals (figure 3). Hence we can assume that the neutrals, which are slow, are generated directly from the heated thin film and the fast component is from ions, as reported from several earlier reports [30, 35]. In the case of femto second

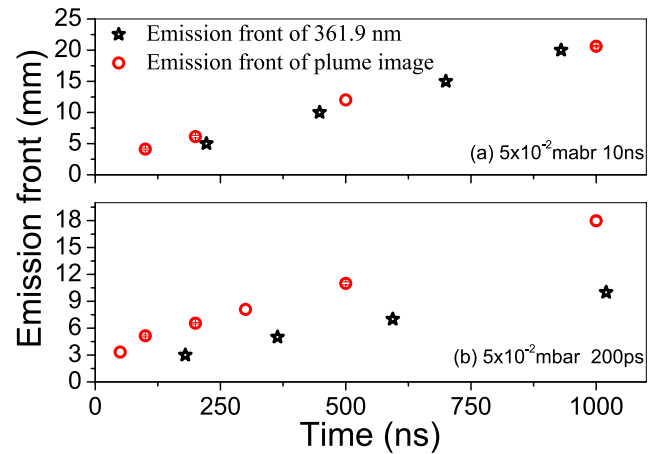


**Figure 4.** Comparison of positional front of neutral line (361.9 nm) emission recorded using spectrometer and PMT with the plume front position estimated from the ICCD image. Nanosecond laser generated plume does not show significant deviations, but the pico second laser generated plume shows significant delay for the neutral species when compared to the plume position front recorded with the camera.

ablated plasma, as can be seen from the TOF as well as from fast imaging, the plume propagates with much slower speed than for the other two cases. Plume volume and the intensity of plume emission are significantly less and in addition to the slower plasma plume, the life time of this plume is also quite short. The time of arrival of neutral emission and that of the plume front from images matches reasonably suggesting the neutrals should be present at plume front. Moreover, the TOF signal corresponding to neutral (figure 3) does not show double peak structure as seen from images indicating that the trailing part of fs generated plume has a different composition as compared to the front portion. The image of plasma plume (figure 2) with extended gate duration (250 ns) shows that the slower component is rather stationary up to  $4 \mu\text{s}$ , indicating the mass of the emitting species should be larger, probably due to clusters or nano-particles [33].

Expansion of the plasma plume in the surrounding medium has been modelled by the blast wave as well as drag force models discussed in the literature [36, 37]. Equation (1) defines the shock position according to the Taylor–Sedov theory of spherical blast wave due to a point explosion.

$$R = \xi_0 \left( \frac{E_0}{\rho_0} \right)^{1/5} t^{2/5} \quad (1)$$

where  $t$  is the delay time,  $\rho_0$  is the density of ambient gas,  $E_0$  is the energy released during explosion.  $\xi_0 = [(75/16\pi)(\gamma - 1)(\gamma + 1)^2/(3\gamma - 1)]^{1/5}$  is a constant with  $\gamma$  the specific heat ratio. The general form of equation (1) used for fitting an  $R$ - $T$  plot is  $R(t) = at^n$  where  $a$  is a constant and  $n = 0.4$  for a perfect spherical shock. In the rear ablation geometry, the mass ablated is significantly large ( $0.4 \mu\text{g}$  for spot size of 1.1 mm diameter, 50 nm thick film assuming the complete ablation of nickel) in comparison to the front ablation (order of nano grams). The limiting distance [36] for the validity of shock wave for the rear ablated mass at 1 mbar is around 5 mm for 1064 nm excitation in case of ns whereas it will be nearly

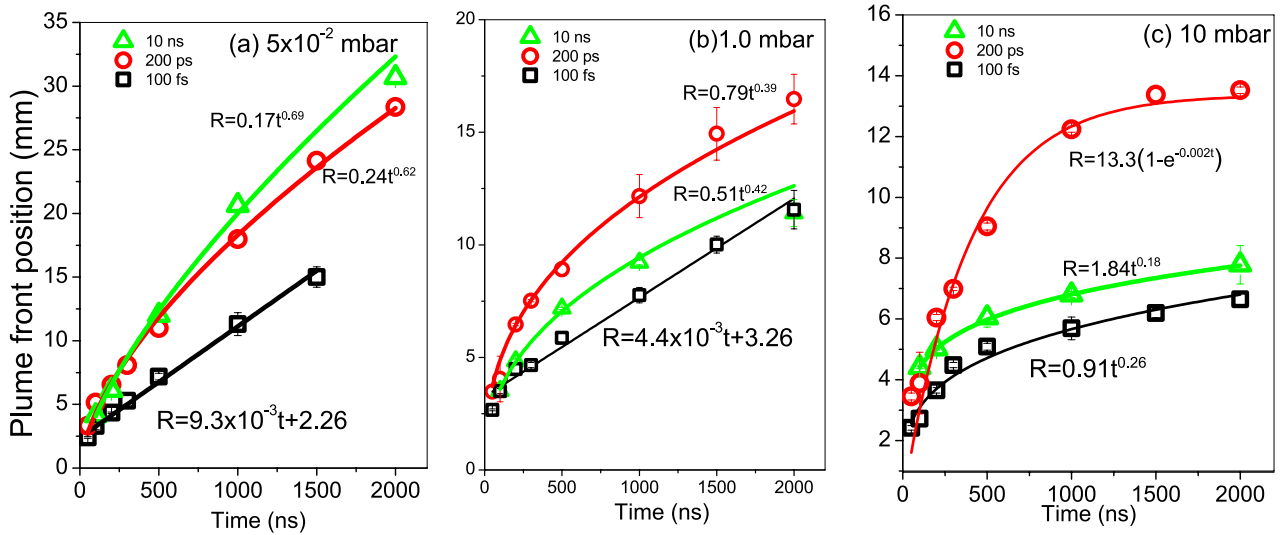


**Figure 5.** Position of the plume front position plotted against time for different laser pulse widths used for each background pressure. The solid lines are the appropriate fits of plasma plume front position with time.

2.2 mm for ps and fs ablations due to the smaller spot size. For a background pressure of  $5 \times 10^{-2}$  mbar, it comes out to be significantly large (few 5–10 cm) whereas at 10 mbar it is less than one mm. Hence, the validity of a perfect shock wave model appears not valid for the pressure of  $5 \times 10^{-2}$  mbar, however in the other two pressures this model can be valid to describe the plume expansion.

In general, the plume expansion in a medium at a later stage can be modeled by the drag model [36, 37] as given in equation (2)

$$R = R_0[1 - \exp(-\beta t)] \quad (2)$$

where  $R_0$  is the stopping distance of the plume and  $\beta$  is the slowing coefficient. This predicts the slowing of plasma plume after a certain distance.

In figure 5 the position of the plasma plume front, estimated from fast imaging is also shown for the corresponding delay times for different pulse widths at each pressure. The figure shows that the plasma plume dynamics is distinctly different and depends on the laser pulse width and background pressure. For instance, in case of fs plume at higher pressure the plume front fits with a blast model with the exponential term as 0.26 suggesting a non-spherical expansion which is also evident from the images (figure 1). From the blast wave model fit to the data, the values of the exponent show a significant deviation from sedovs theory [38], which is in line with the observation by other groups as well [36]. A possible reason for this deviation may be the experimental geometry, where the melted mass can-not readily expand to the surrounding gas medium due to finite thickness of the film. Also, it may be mentioned here that the interaction of ultra fast laser with metal leads to nano particle formation as reported earlier [33], which are heavy in size and will not be affected significantly by the buffer gas. At lower background pressures plume expansion fits to a linear expansion with a velocity of  $4.4 \times 10^5$  cm s $^{-1}$  and  $9.3 \times 10^5$  cm s $^{-1}$  for 1.0 mbar and  $5 \times 10^{-2}$  mbar respectively.

Similarly for ps laser plasma plume at higher pressure (10 mbar), the plasma plume shows a drag type behavior

with stopping distance of 13.3 mm and slowing constant of  $0.002$  ns $^{-1}$ . However, a blast model fits at lower pressures of 1 mbar and  $5 \times 10^{-2}$  mbar. Blast model fit at 1 mbar and the exponent value of 0.39 suggests a nearly spherical expansion of the shock front [39]. In this case the plume front position is in a region where the shock wave model can be applied as the plume propagates above the minimum limiting distance for the validity of shock modeling (2.2 mm for 1 mbar at 0.8 mm dia spot size). However, in case of  $5 \times 10^{-2}$  mbar, though the plume front position is not in the limiting region ( $>5$  cm) of shock wave, the plasma plume front position is showing a shock like expansion with time exponent value of 0.62, of course, much deviated from the spherical shock. Also, the constant multiplier value is also significantly less as compared to that at 1 mbar. Similarly, in the case of ns ablation also, at  $5 \times 10^{-2}$  mbar, the plasma plume front position shows a blast wave model like expansion (though not valid) with  $R = 0.17 \times t^{0.69}$  which is similar to that in ps case.

However, as the background pressure increases to 1.0 mbar, where the shock model is applicable in the present case, the data fit well with a shock model with time exponent of 0.42, which is again suggestive of a spherical shock. When the background pressure increases further to 10.0 mbar, the plume front again shows the trajectory of a shock model with significantly deviated time exponent (0.18) and higher multiplier factor compared to other pressures and pulse widths. In summary, at a pressure of  $5 \times 10^{-2}$  mbar (figure 5(a)) plume expansion shows a linear behaviour for fs ablation, which changes its nature to a shock like expansion for ps and ns ablations. At 1 mbar background pressure (figure 5(b)) also the fs ablation shows a linear expansion, however, a good spherical shock like expansion with time exponent value near to 0.4 is observed for the ps and ns ablation. As the pressure increases further to 10 mbar (figure 5(c)), the fs and ns ablations show a shock wave like nature however, the ps ablation shows a clear drag like trend in its propagation.

The role of film thickness in plume expansion dynamics becomes more prominent when the laser pulse is shorter. For

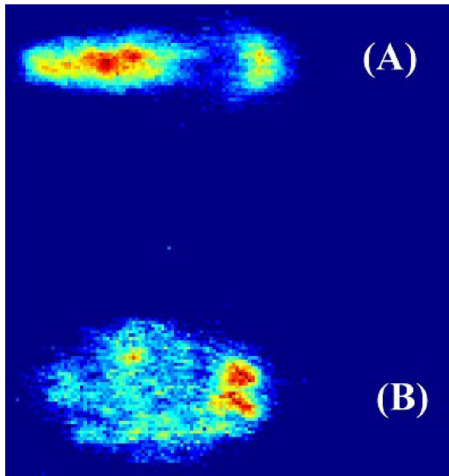


**Figure 6.** Images of plasma plume generated by successive 100 fs laser pulses irradiating the same spot of the film (recorded 1  $\mu$ s after excitation). (A) Plume after the first pulse, (B) plume after the second pulse on the same spot.

instance, the expansion of the 200 ps plasma plume is significantly different from that of the 10 ns plume, as the former shows a high directionality. Moreover, the plume shows a focusing behaviour at about 500 ns during expansion. Laser plume focusing has been explained well by Bulgakova [40] using the analogy of an under-expanded jet, which should be a reasonable assumption in our case also.

Here it can be mentioned that more detailed work and modeling may be needed to explain why drag-like model is a better fit for the 200 ps plume dynamics. However, as discussed, 100 fs plume shows a highly directional expansion, and the plume front does not fit either with the blast model or the drag model at lower pressures. Rather, at lower pressure, the plume shows a linear dependence with time, like free expansion, as shown in figure 5. The plume intensity is very small compared to the plumes formed by nanosecond and picosecond pulses. This low intensity could be the result of the lesser ablated mass and/or smaller number of excited species in the plume as a result of nano particle or cluster formation as mentioned earlier.

The aspect ratio of the expanding plume remains almost constant with nanosecond pulse excitation, similar to that reported previously for LPP experiments in solid targets [41]. This is in contrast to the earlier LBO results from 55 micron thick LiFC samples [3], where the plume was shown to have a directional nature. The possible reason for this change in plume expansion dynamics could be decreased thickness of the sample used for ablation, as complete meltdown of the irradiated spot is possible. In laser-matter interaction, the plasma corona formation time is important as it decides the probability of laser absorption by critical density plasma. For effective laser absorption to happen, the laser pulse width should be either comparable or more than the corona formation time depending on the laser power density and the irradiation spot size [42]. In the case of 10 ns and 200 ps laser ablation the calculated corona formation times comes out as 1.12 ns and 410 ps respectively. This suggests that the plume may absorb part of laser energy in either case, with more probability of absorption for nanosecond ablation. Moreover, the

LBO geometry can restrict plume expansion due to significant melt-through time required for the film to melt, which will delay corona formation even further. Therefore, in the case of nanosecond ablation, the thin film at the point of irradiation melts completely before the termination of the laser pulse, and corona plasma is formed which absorbs the trailing part of the laser pulse, so that the expansion is almost similar to that of an LPP plume.

It may be noted that compared to 100 fs pulse ablation, the intensity of the fast component is relatively higher as compared to the plume formed from 200 ps pulse ablation. Images reveal that the plume splits into two components during initial 500 ns. As mentioned earlier, plume brightness, directionality and lifetime are found to be critically dependent on the laser pulse width. For instance, the ablated mass and plume lifetime increase with the pulse width. Furthermore, ps and fs pulses produce directional plumes, in agreement with certain earlier ns LBO experiments done on films [3] with larger thickness.

Another important aspect of laser-solid interaction is the plasma pressure created due to heating causes matter to blow off at the sound speed of  $C_s = \sqrt{\frac{Z^* k_B T_e}{m_i}}$  where  $Z^*$  is the effective ion charge,  $T_e$  is the electron temperature,  $k_B$  is the Boltzmann constant, and  $m_i$  is the ion mass. However, considering the modeling [24, 43] used for the ablation of ultra fast lasers on metals, the penetration depth can be estimated based on the electron thermal diffusion length  $l_{th}^e \approx (D_e \tau_e)^{1/2}$  where  $D_e = K_e / C_e$  is the electron diffusion coefficient and  $\tau_e$  corresponds to energy relaxation time of electrons which is approximately  $\approx 1$  ps for metals. For nickel, the electron thermal conductivity can be estimated as  $K_e = K_0 T_e / T_i$  where  $K_0 = 91 \text{ W m}^{-1} \text{ K}^{-1}$  and the electron heat capacity  $C_e = \gamma T_e$ , with  $\gamma = 1065 \text{ J m}^{-3} \text{ K}^{-2}$  [44]. If we assume room temperature for electrons and lattice, then  $l_{th}^e$  estimated using the above mentioned equations and constants is comes out  $\approx 18 \text{ nm}$ . In case of laser pulses with widths significantly longer than  $\tau_e$ , the lattice will continue to get energy for melting up to the laser pulse duration and hence the electron thermal diffusion length can be assumed as  $l_{th}^e \approx (D_e \tau_L)^{1/2}$  where  $\tau_L$  is the laser pulse width. In the present case this leads to 1.6  $\mu$  m and 240 nm for 10 ns and 200 ps pulse widths respectively. It can be noted that this estimation is based on the assumption that both lattice and electrons are at room temperature. However, this assumption of room temperature for lattice and electron can not be valid in case of (i) the presence of pre pulses which affect the lattice temperature before the fs pulse interacts with film, (ii) long duration of the ns and ps pulses changes lattice temperature during the melting process. If we expect that the lattice gets heated to nearly the melting point of nickel (1745 K), either by means of the pre pulse or the front portion of longer pulses,  $l_{th}^e$  comes out 7 nm, 200 nm and 700 nm for fs, ps and ns pulses respectively. Nonetheless, from the modeling, considering 50 nm thick free standing thin film of nickel [24, 43] with the parameters similar to our experimental conditions, for fs ablation, the optical penetration is  $\approx 14 \text{ nm}$ , which agrees with the estimated value from the present experiment.



As mentioned above, the thickness of the molten layer formed by laser irradiation can be decided by the laser pulse duration. In case of ns pulse the entire film may get melted while the laser pulse is on whereas for the fs laser ablation only a small portion of the film melts during the pulse duration. Thus, in the present scenario of rear ablation/LBO geometry, pressure build up will be huge as the melt gets sandwiched between the quartz surface in the back and a layer of still un-melted film in the front. The tensile strength of the un-melted film can result in strong confinement of the high temperature molten material. The tensile strength decreases in time due to thermal conduction and melting of the film and hence the pressure propels the molten material in the forward direction. As temperature and pressure gradients are not very steep and by the time peak pressure builds up (towards the trailing edge of the laser pulse), the tensile strength would be reduced and the entire film at the point of irradiation transform into a semi-molten stage. The molten material will expand outwards into the surrounding medium much similar to the LPP/front ablation. It is the decreased film thickness in comparison to the earlier rear ablation works [45] that may be responsible for the plasma plume expansion behave more like that in the case of LPP expansion. Even though the surface temperatures and pressures achieved for ultra short pulses will be relatively much higher [44] due to shorter optical penetration, the plume expulsion will be less compared to nanosecond excitation, as is evident from our observations. Also, the significant portion of the un-melted film in case of fs ablation, makes the plume expand slowly akin to thermal formation of plasma plume as can be seen in the fitting of plasma plume front position with time (figure 5).

To check whether a single 100 fs laser pulse can ablate the entire irradiated region, we irradiated the same spot of the film twice in succession. Significant plume formation is found for both the pulses, which shows that the ultra fast laser pulse (of the used energy density and power density) could not ablate the irradiated film surface completely in the first shot. However a third pulse on the same spot resulted in no plume, confirming that the irradiated spot was completely ablated after the second pulse (to check if substrate contributed to the plume we checked the substrate surface with a simple optical microscope after ablation, and no noticeable damage was seen on the substrate).

This portion melts thereafter due to the deposited energy and expels the molten material to the surroundings, akin to a jet from a nozzle. The portion of the film where the central part of the Gaussian laser beam is incident melts faster and acts as an orifice for the jet. This nozzle effect makes the plume propagate in unidirectional fashion. In the case of femtosecond ablation the melted material rapidly cools and part of it sticks back to the substrate, through re-solidification of the melted plume [46]. The re-solidification time scale is estimated as sub nanosecond, hence it is not a favorable scenario in case of rear ablation for longer pulse widths. However, for pulses with much shorter duration than the re-solidification time, the chances of the melted plume sticking back to the substrate

are there. The re-solidification process, lesser melting of thin film and the ejection of plume as a jet results in the reduction in plume volume compared to the plume formed with longer pulses. Plume generation by the second pulse is a confirmation for the sticking back of melted species to the substrate. Figure 6 shows the plume images recorded for the successive first and second laser pulses irradiating the same spot for a background pressure of 1 mbar. The relatively large divergence of the plume generated by the second pulse indeed confirms the occurrence of nozzle effect for the first pulse, and explains the directionality. However, plume formation is not observed with a second pulse in case of ns and ps pulses.

Here we would like to mention that significant amount of studies in the field of laser interaction on different materials evolved in the form of experiment and modeling [47]. As mentioned earlier the present study will be important from the view point its manifold applications, e.g. thin film deposition, cleaning of objects, etc [23–26].


#### 4. Conclusion

In conclusion, we have experimentally generated rear ablation (LBO) plasmas by irradiating a thin Ni target with long as well as ultra-short laser pulses, and studied their expansion in a nitrogen atmosphere. When excited with 10 ns pulse, the generated plasma does not show any evidence of plume focusing or splitting, and behaves as if the plume is generated from a solid sample in the front ablation/LPP geometry. On the other hand, the plume formed from 200 picosecond laser distinctly shows plume focusing in the initial phase followed by the splitting of the plume in the later part of the expansion. Plume with 100 fs pulses shows an early plume splitting and also a highly directional nature.

Further, we report some interesting insights into the interaction of intense laser pulses with thin films in the rear ablation (LBO) geometry, and the effect of laser pulse width on plume formation and its propagation in the ambient gas. For fs ablation, temporal dynamics of plasma plume is explained considering an analogy with the expulsion of molten matter through a nozzle, where the film thickness and pulse width define the nozzle parameters. The propagation shows a distinct behavior depending on the laser pulse width. It is also evident that the plume formation mechanism may be instrumental in deciding the plume expansion dynamics. Relevant models are discussed to explain the salient features of the observations. We believe the present study may have potential implications in pulsed laser deposition, ultra fast laser based nano particle generation and micro-machining.

#### ORCID iDs

Jinto Thomas  <https://orcid.org/0000-0003-0672-7203>

Hem Chandra Joshi  <https://orcid.org/0000-0001-9518-2473>

Reji Philip  <https://orcid.org/0000-0003-3836-470X>



## References

- [1] Nolte S, Momma C, Jacobs H, Tünnermann A, Chichkov B N, Wellegehausen B and Welling H 1997 *J. Opt. Soc. Am. B* **14** 2716–22
- [2] Hubler G K and Chrisey D B 1994 *Pulsed Laser Deposition of Thin Films* (New York: Wiley)
- [3] Kumar A, George S, Singh R and Nampoori V 2010 *Laser Part. Beams* **28** 387–92
- [4] Yeates P and Kennedy E T 2010 *J. Appl. Phys.* **108** 093306
- [5] Purvis M A, Grava J, Filevich J, Ryan D P, Moon S J, Dunn J, Shlyaptsev V N and Rocca J J 2010 *Phys. Rev. E* **81** 036408
- [6] Amoroso S, Bruzzese R, Wang X, Nedialkov N N and Atanasov P A 2007 *J. Phys. D: Appl. Phys.* **40** 331
- [7] LaHaye N L, Harilal S S, Diwakar P K and Hassanein A 2013 *J. Anal. At. Spectrom.* **28** 1781–7
- [8] Anoop K K, Harilal S S, Philip R, Bruzzese R and Amoroso S 2016 *J. Appl. Phys.* **120** 185901
- [9] Mattioli M, Giannella R, Myrnas R, Demichelis C, Denne-Hinnov B, Dudok DeWit T and Magyar G 1995 *Nucl. Fusion* **35** 1115–24
- [10] Brezinsek S, Huber A, Jachmich S, Pospieszczyk A, Schweer B and Sergienko G 2005 *Fusion Sci. Technol.* **47** 209–19
- [11] Reinke M L, Beiersdorfer P, Howard N T, Magee E W, Podpaly Y, Rice J E and Terry J L 2010 *Rev. Sci. Instrum.* **81** 10D736
- [12] Fardel R, Nagel M, Nesch F, Lippert T and Wokaun A 2007 *Appl. Phys. Lett.* **91** 061103
- [13] Kumar A, Singh R K, Subramanian K P, Patel B G, Sunil S and Prajapati I A 2006 *J. Phys. D: Appl. Phys.* **39** 4860
- [14] Singh R K, Kumar A, Prahlad V and Joshi H C 2008 *Appl. Phys. Lett.* **92** 171502
- [15] Anisimov S I and Luk'yanchuk B S 2002 *Phys.—Usp.* **45** 293–324
- [16] Roy A, Harilal S S, Polek M P, Hassan S M, Endo A and Hassanein A 2014 *Phys. Plasmas* **21** 033109
- [17] Freeman J, Harilal S, Diwakar P, Verhoff B and Hassanein A 2013 *Spectrochim. Acta B* **87** 43–50
- [18] Rousse A et al 2001 *Nature* **410** 65–7
- [19] Roeterdink W G, Juurlink L B F, Vaughan O P H, Dura Diez J, Bonn M and Kleyn A W 2003 *Appl. Phys. Lett.* **82** 4190–2
- [20] Zhang Z, VanRompay P A, Nees J A and Pronko P P 2002 *J. Appl. Phys.* **92** 2867–74
- [21] Varier G, Issac R, Harilal S, Bindhu C, Nampoori V and Vallabhan C 1997 *Spectrochim. Acta B* **52** 657–66
- [22] Wang W, Jiang G, Mei X, Wang K, Shao J and Yang C 2010 *Appl. Surf. Sci.* **256** 3612–7
- [23] Pabst L, Ullmann F, Ebert R and Exner H 2018 *Appl. Phys. A* **124** 241
- [24] Saito T, Matsuda O and Wright O B 2003 *Phys. Rev. B* **67** 205421
- [25] Li X, Jiang L and Tsai H L 2009 *J. Appl. Phys.* **106** 064906
- [26] Bilmes G M, Vallejo J, Vera C C and Garcia M E 2018 *Appl. Phys. A* **124** 347
- [27] Thomas J, Joshi H C, Kumar A and Philip R 2018 *Phys. Plasmas* **25** 103108
- [28] Kumar A, Singh R K, Thomas J and Sunil S 2009 *J. Appl. Phys.* **106** 043306
- [29] Geohegan D B and Poretzky A A 1995 *Appl. Phys. Lett.* **67** 197–9
- [30] Anoop K K, Ni X, Wang X, Amoroso S and Bruzzese R 2014 *Laser Phys.* **24** 105902
- [31] Anoop K K, Ni X, Bianco M, Paparo D, Wang X, Bruzzese R and Amoroso S 2014 *Appl. Phys. A* **117** 313–8
- [32] Yadav D, Gupta V and Thareja R K 2009 *J. Appl. Phys.* **106** 064903
- [33] Amoroso S, Ausanio G, Bruzzese R, Gagnaniello L, Lanotte L, Vitiello M and Wang X 2006 *Appl. Surf. Sci.* **252** 4863–70
- [34] Kramida A, Ralchenko Y, Reader J and NIST ASD Team 2018 *NIST Atomic Spectra Database (ver. 5.5.6)* (Gaithersburg, MD: National Institute of Standards and Technology) (<https://physics.nist.gov/asd>) (Accessed: 4 July 2018)
- [35] Wu J, Li X, Wei W, Jia S and Qiu A 2013 *Phys. Plasmas* **20** 113512
- [36] Sharma A K and Thareja R K 2005 *Appl. Surf. Sci.* **243** 68–75
- [37] Schmitz T A, Koch J, Gnther D and Zenobi R 2011 *J. Appl. Phys.* **109** 123106
- [38] Li Y T, Zhang J, Teng H, Li K, Peng X Y, Jin Z, Lu X, Zheng Z Y and Yu Q Z 2003 *Phys. Rev. E* **67** 056403
- [39] Freiwald D A and Axford R A 1975 *J. Appl. Phys.* **46** 1171–4
- [40] Bulgakov A V and Bulgakova N M 1998 *J. Phys. D: Appl. Phys.* **31** 693
- [41] Harilal S S, Bindhu C V, Tillack M S, Najmabadi F and Gaeris A C 2003 *J. Appl. Phys.* **93** 2380–8
- [42] Atzeni S 2000 *Plasma Phys. Control. Fusion* **42** B143–55
- [43] Ivanov D S and Zhigilei L V 2003 *Phys. Rev. B* **68** 064114
- [44] Hohlfeld J, Wellershoff S S, Gdde J, Conrad U, Jhnke V and Matthias E 2000 *Chem. Phys.* **251** 237–58
- [45] Kumar A, Singh R K, Prahlad V and Joshi H C 2008 *J. Appl. Phys.* **104** 093302
- [46] Fang R, Vorobyev A and Guo C 2017 *Light-Sci. Appl.* **6** e16256
- [47] Nedialkov N, Atanasov P, Amoroso S, Bruzzese R and Wang X 2007 *Appl. Surf. Sci.* **253** 7761–6